PNAS RESEARCH ARTICLE | NEUROSCIENCE

SIK3–HDAC4 in the suprachiasmatic nucleus regulates the timing of arousal at the dark onset and circadian period in mice

Fuyuki Asano[a], Staci J. Kim[a], Tomoyuki Fujiyama[a], Chika Miyoshi[a], Noriko Hotta-Hirashima[a], Nodoka Asama[a], Kanako Iwasaki[a], Miyo Kakizaki[a], Seiya Mizuno[b], Michihiro Mieda[c], Fumihiro Sugiyama[b], Satoru Takahashi[b], Shoi Shi[a], Arisa Hirano[a,d], Hiromasa Funato[a,e,1], and Masashi Yanagisawa[a,f,g,1]

Contributed by Masashi Yanagisawa; received October 27, 2022; accepted February 7, 2023; reviewed by Yoshitaka Fukada and Louis Ptáček

Mammals exhibit circadian cycles of sleep and wakefulness under the control of the suprachiasmatic nucleus (SCN), such as the strong arousal phase-locked to the beginning of the dark phase in laboratory mice. Here, we demonstrate that salt-inducible kinase 3 (SIK3) deficiency in gamma-aminobutyric acid (GABA)-ergic neurons or neuromedin S (NMS)–producing neurons delayed the arousal peak phase and lengthened the behavioral circadian cycle under both 12-h light:12-h dark condition (LD) and constant dark condition (DD) without changing daily sleep amounts. In contrast, the induction of a gain-of-function mutant allele of *Sik3* in GABAergic neurons exhibited advanced activity onset and a shorter circadian period. Loss of SIK3 in arginine vasopressin (AVP)–producing neurons lengthened the circadian cycle, but the arousal peak phase was similar to that in control mice. Heterozygous deficiency of histone deacetylase (HDAC) 4, a SIK3 substrate, shortened the circadian cycle, whereas mice with HDAC4 S245A, which is resistant to phosphorylation by SIK3, delayed the arousal peak phase. Phase-delayed core clock gene expressions were detected in the liver of mice lacking SIK3 in GABAergic neurons. These results suggest that the SIK3–HDAC4 pathway regulates the circadian period length and the timing of arousal through NMS-positive neurons in the SCN.

SIK3 | HDAC4 | circadian rhythms | circadian period | arousal timing

Significance

Sleep homeostasis and circadian rhythm are well-established processes for sleep regulation. The serine/threonine kinase SIK3 is reported as a key molecule for sleep homeostasis. Here, we found that SIK3 in the suprachiasmatic nucleus, the brain's master pacemaker region, is involved in the determination of circadian period length and the arousal timing at the dark onset, without affecting sleep amount and pressure. Our studies suggest that the SIK3–HDAC4 pathway plays a critical role in sleep regulation through both circadian rhythm and sleep homeostasis.

Animals show daily changes in physiology and behavior to adapt to the 24-h environmental light–dark cycle with an activity peak at specific circadian timing. C57BL/6 mice exhibit nocturnal behavior with strong arousal for several hours immediately after the onset of the dark phase, which is sustained under constant darkness by the endogenous circadian clock. The suprachiasmatic nucleus (SCN) in the hypothalamus serves as the master circadian pacemaker that synchronizes the peripheral clocks of the whole body (1–4). The SCN consists of two subdivisions, the core (or a ventrolateral region) and the shell (or a dorsolateral region), which are composed of distinct groups of gamma-aminobutyric acid (GABA)-ergic neurons characterized by the expression of neuropeptides. Neuromedin S (NMS)–producing neurons account for 40% of SCN neurons and are distributed in both the core and shell regions. NMS-positive neurons have a dominant role in determining the circadian length of the SCN and behavior (5, 6). Arginine vasopressin (AVP)–producing neurons exist in the shell region and regulate behavioral rhythms and susceptibility to a jet lag (7–11). Vasoactive intestinal peptide (VIP)–producing neurons are localized in the core region, and VIP-producing neurons are required for the synchronization of SCN neuron activity and behavioral rhythm regulation (1–4). In addition to generating internal timing, the SCN is important for sleep and wakefulness to occur at specific times of the day, such as the rapid and robust increase in arousal at the onset of the dark period in mice (12). VIP-producing neurons are involved in nighttime sleep, "siesta" (13). The transcriptional–translational feedback loop that consists of transcriptional activators, CLOCK and BMAL1, and two repressors, PERIOD and CRYPTOCHOROME, serves as the molecular basis of 24-h molecular oscillation (14). We have reported salt-inducible kinase (SIK) 3 as a positive regulator of sleep pressure (15–17). Loss of a conserved protein kinase A phosphorylation site in SIK3 leads to an increase in nonrapid eye movement sleep (NREMS) amount and electroencephalogram (EEG) delta power during NREMS. In addition to sleep pressure regulation, SIK3 may be involved in circadian behavior since SIK3-deficient mice showed a longer circadian period (18). However, more than 90% of salt-inducible kinase 3 (SIK3)-deficient mice died on the first day after birth, and the surviving few showed growth retardation and developed multiple metabolic and skeletal abnormalities (19, 20). Thus, to precisely investigate the role of SIK3 in circadian behavior,

Author contributions: F.A., H.F., and M.Y. designed research; F.A., S.J.K., T.F., C.M., N.H.-H., N.A., K.I., and M.K. performed research; F.A., T.F., C.M., S.M., M.M., F.S., and S.T. contributed new reagents/analytic tools; F.A., S.S. and A.H. analyzed data; and F.A., H.F., and M.Y. wrote the paper.

Reviewers: Y.F., University of Tokyo; and L.P., University of California San Francisco.

The authors declare no competing interest.

[1]To whom correspondence may be addressed. Email: funato.hiromasa.km@u.tsukuba.ac.jp or yanagisawa.masa.fu@u.tsukuba.ac.jp.

This article contains supporting information online at https://www.pnas.org/lookup/suppl/doi:10.1073/pnas.2218209120/-/DCSupplemental.

Published March 6, 2023.

it is necessary to manipulate of SIK3 specific to SCN neuron groups.

In this study, we used *Sik3*^{flox} mice, which exhibit SIK3 deficiency depending on a Cre recombinase and examined sleep and circadian behaviors in mice deficient in SIK3 in GABAergic neurons, NMS-positive neurons, and AVP-positive neurons. *Vgat*$^{Cre/+}$*; Sik3*$^{flox/flox}$ and *Nms-Cre; Sik3*$^{flox/flox}$ mice showed a longer period length and delayed activity onset at the beginning of the dark phase. In contrast, *Avp-Cre; Sik3*$^{flox/flox}$ mice had a longer period length with normal arousal at the dark phase onset. We also found that histone deacetylase 4 (HDAC4), one of the well-established phosphorylation targets of SIK3, regulates the circadian period and peak phase of arousal. These results indicate that the SIK3–HDAC4 pathway in the NMS-positive neurons regulates circadian period length and arousal timing, but the contribution may differ among subpopulations of the NMS-positive neurons.

Results

SIK3 Deficiency in GABAergic Neurons Caused a Delayed Arousal Peak and a Longer Circadian Period. Through the course of EEG/electromyogram (EMG)-based sleep analysis of SIK3 deficiency in specific neuron subtypes, we noticed that *Vgat*$^{Cre/+}$*; Sik3*$^{flox/flox}$ mice showed a delayed arousal peak after the beginning of the dark phase (*SI Appendix*, Fig. S1*A*). Whereas control mice exhibited a steep increase in arousal around light-off at ZT12 (onset of peak arousal in a 3-h range at zeitgeber time (ZT) 11.5 ± 0.1), *Vgat*$^{Cre/+}$*; Sik3*$^{flox/flox}$ mice showed a gradual increase during the dark phase, reaching a peak at ZT15.1 ± 0.6 (Fig. 1 *A*–*C*). Hourly NREM

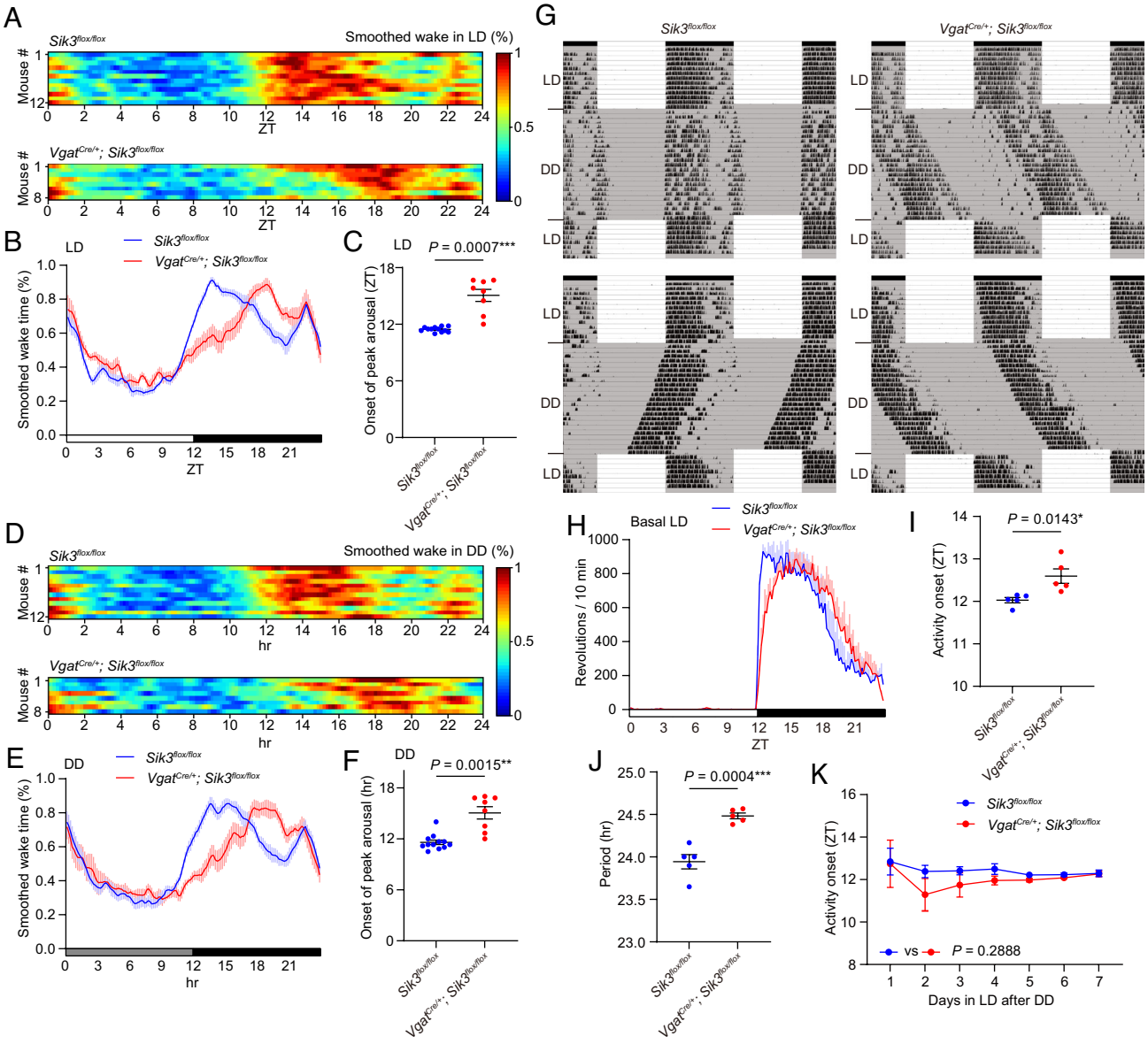

Fig. 1. *Vgat*$^{Cre/+}$*; Sik3*$^{flox/flox}$ mice showed phase-delayed awakening at the dark onset and a longer circadian period (*A*) Heat maps of smoothed wake time of individual *Sik3*$^{flox/flox}$ mice and *Vgat*$^{Cre/+}$*; Sik3*$^{flox/flox}$ mice in LD. (*B*) Mean of smoothed wake time of *Vgat*$^{Cre/+}$*; Sik3*$^{flox/flox}$ mice in LD. (*C*) The onset of peak arousal of *Vgat*$^{Cre/+}$*; Sik3*$^{flox/flox}$ mice in LD. Welch's *t* test. (*D*) Heat maps of smoothed wake time of individual *Sik3*$^{flox/flox}$ mice and *Vgat*$^{Cre/+}$*; Sik3*$^{flox/flox}$ mice on the first day in DD. (*E*) Mean of smoothed wake time of *Vgat*$^{Cre/+}$*; Sik3*$^{flox/flox}$ mice in the first day in DD. (*F*) The onset of peak arousal of *Vgat*$^{Cre/+}$*; Sik3*$^{flox/flox}$ mice in the first day in DD. Welch's *t* test. (*G*) Representative double plots of running-wheel activity of a *Sik3*$^{flox/flox}$ mouse and a *Vgat*$^{Cre/+}$*; Sik3*$^{flox/flox}$ mouse. (*H*) Daily wheel revolutions per 10 min of *Vgat*$^{Cre/+}$*; Sik3*$^{flox/flox}$ mice in basal LD. (*I*) Activity onset of *Vgat*$^{Cre/+}$*; Sik3*$^{flox/flox}$ mice in basal LD. Welch's *t* test. (*J*) Circadian period of *Vgat*$^{Cre/+}$*; Sik3*$^{flox/flox}$ mice. Unpaired *t* test. (*K*) Estimated activity onset of *Vgat*$^{Cre/+}$*; Sik3*$^{flox/flox}$ mice during the reentrainment LD period after DD. Two-way repeated measure ANOVA. For *A*–*F*, *Vgat*$^{Cre/+}$*; Sik3*$^{flox/flox}$ mice (n = 8) and *Sik3*$^{flox/flox}$ mice (n = 12) were used. For *G*–*K*, n = 5 for each genotype was used. Data are mean ± SEM.

sleep time and REMS time of *Vgat*$^{Cre/+}$; *Sik3*$^{flox/flox}$ mice showed a gradual decrease during the dark phase which was complementary to increased wake time (*SI Appendix*, Fig. S1 *B* and *C*). In addition to the highest peak of arousal at the early dark phase, C57BL6 mice showed a second and lower peak of arousal at the end of the dark phase. *Vgat*$^{Cre/+}$; *Sik3*$^{flox/flox}$ mice show no delay from control mice for this arousal peak (Fig. 1 *A* and *B*). *Vgat*$^{Cre/+}$; *Sik3*$^{flox/flox}$ mice exhibited total wake time, total NREMS time, total REMS time, mean episode duration of NREMS, and delta power in NREMS similar to control mice (*SI Appendix*, Fig. S1 *D–H*). Thus, the only significant abnormality in sleep/wakefulness in *Vgat*$^{Cre/+}$; *Sik3*$^{flox/flox}$ mice was a delayed peak of arousal in the early dark phase.

To examine whether light, either as a zeitgeber signal or through the extended masking effect, causes a delayed arousal peak in *Vgat*$^{Cre/+}$; *Sik3*$^{flox/flox}$ mice, we performed sleep/wake analysis using the first day in DD. As in LD, control mice exhibited a steep increase in arousal around the end of the subjective day (11.6 ± 0.3 h later at the end of the dark phase) (Fig. 1 *D–F*). However, *Vgat*$^{Cre/+}$; *Sik3*$^{flox/flox}$ mice showed a gradual increase in arousal, reaching a peak at 15.1 ± 0.7 h (Fig. 1 *D–F*). In DD, *Vgat*$^{Cre/+}$; *Sik3*$^{flox/flox}$ mice exhibited total wake time, total NREMS time, total REMS time, mean episode duration of NREMS, and delta power in NREMS similar to control mice (*SI Appendix*, Fig. S1 *I–P*). Thus, SIK3 deficiency in GABAergic neurons caused a phase-delayed arousal peak under both LD and DD.

Next, we examined the circadian behavior of *Vgat*$^{Cre/+}$; *Sik3*$^{flox/flox}$ mice using a running wheel. *Vgat*$^{Cre/+}$; *Sik3*$^{flox/flox}$ mice exhibited a longer circadian period under DD (*Sik3*$^{flox/flox}$ mice: 23.9 ± 0.1 h and *Vgat*$^{Cre/+}$; *Sik3*$^{flox/flox}$ mice: 24.5 ± 0.0 h, $P = 0.0004$; Fig. 1 *G* and *J*). Consistent with a delayed arousal peak in the early dark phase in both LD and DD, *Vgat*$^{Cre/+}$; *Sik3*$^{flox/flox}$ mice exhibited a delayed or variable activity onset after the beginning of the dark phase in LD (Fig. 1 *G–I*). The number of wheel revolutions of *Vgat*$^{Cre/+}$; *Sik3*$^{flox/flox}$ mice was reduced later in the dark phase compared to that of *Sik3*$^{flox/flox}$ mice (Fig. 1*H*). When LD was resumed at the original circadian timing after DD, activity onset of *Vgat*$^{Cre/+}$; *Sik3*$^{flox/flox}$ mice was immediately adjusted to the dark phase of LD, as did *Sik3*$^{flox/flox}$ mice (Fig. 1 *G* and *K*). In the first few days of LD, *Vgat*$^{Cre/+}$; *Sik3*$^{flox/flox}$ mice showed an activity peak immediately after the beginning of the dark phase similar to *Sik3*$^{flox/flox}$ mice. Since ZT12 on the first day of the LD corresponded to the subjective dark phase on the last day of DD, this result indicates an intact masking effect of light in *Vgat*$^{Cre/+}$; *Sik3*$^{flox/flox}$ mice. Delayed activity onset reappeared after the fifth day after the resumption of LD (Fig. 1*G*). To further examine the adaptation of *Vgat*$^{Cre/+}$; *Sik3*$^{flox/flox}$ mice to light–dark cycle shift, light-on timing was advanced by 6 h (21). *Vgat*$^{Cre/+}$; *Sik3*$^{flox/flox}$ mice started their activity earlier each day and were entrained to the 6-h advanced LD in 10 d (*SI Appendix*, Fig. S2 *A* and *B*). Daily advances in activity onset were similar for both *Vgat*$^{Cre/+}$; *Sik3*$^{flox/flox}$ and *Sik3*$^{flox/flox}$ mice (*SI Appendix*, Fig. S2*C*). When light-off timing was delayed for 6 h, the activity onset of *Vgat*$^{Cre/+}$; *Sik3*$^{flox/flox}$ mice was immediately shifted to the beginning of the new dark phase, as did control mice. This was likely due to a masking response to light during the dark phase of the previous LD. Delayed activity peak in *Vgat*$^{Cre/+}$; *Sik3*$^{flox/flox}$ mice reappeared after the fourth day after the start of the 6-h delayed LD (*SI Appendix*, Fig. S2*A*). These results indicate that SIK3 deficiency in GABAergic neurons induced a longer circadian period and phase-delayed activity/wake during the early dark phase, with almost intact entrainment to light–dark cycle shift and masking response to light.

***Sleepy* Allele Induction in GABAergic Neurons Advanced Activity Onset and Shortened Circadian Period.** In contrast to a loss-of-function effect examined using *Sik3*^{flox} mice, *Sik3*$^{Slp\text{-}flox}$ mice induce the gain-of-function allele, *Sleepy* (*Slp*), in a Cre recombinase–dependent manner (17). In wheel-running experiments, *Vgat*$^{Cre/+}$; *Sik3*$^{Slp\text{-}flox/Slp\text{-}flox}$ mice exhibited advanced activity onset compared to *Sik3*$^{Slp\text{-}flox/Slp\text{-}flox}$ mice (Fig. 2 *A–C*). In DD, *Vgat*$^{Cre/+}$; *Sik3*$^{Slp\text{-}flox/}$

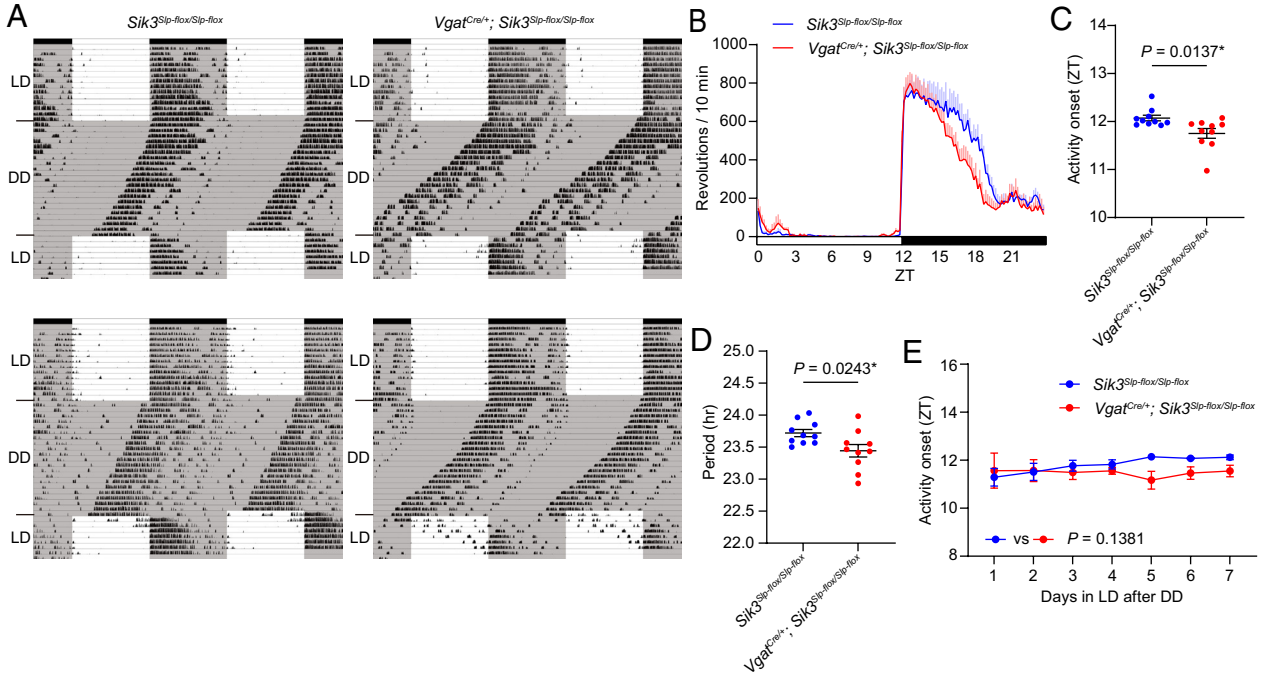

Fig. 2. *Vgat*$^{Cre/+}$; *Sik3*$^{Slp\text{-}flox/Slp\text{-}flox}$ mice showed a shorter circadian period (*A*) Representative double plots of running-wheel activity of a *Sik3*$^{Slp\text{-}flox/Slp\text{-}flox}$ mouse and a *Vgat*$^{Cre/+}$; *Sik3*$^{Slp\text{-}flox/Slp\text{-}flox}$ mouse. (*B*) Daily wheel revolutions per 10 min of *Vgat*$^{Cre/+}$; *Sik3*$^{Slp\text{-}flox/Slp\text{-}flox}$ in basal LD. (*C*) Activity onset of *Vgat*$^{Cre/+}$; *Sik3*$^{Slp\text{-}flox/Slp\text{-}flox}$ mice in basal LD. Unpaired *t* test. (*D*) Circadian period of *Vgat*$^{Cre/+}$; *Sik3*$^{Slp\text{-}flox/Slp\text{-}flox}$ mice. Unpaired *t* test. (*E*) Estimated activity onset of *Vgat*$^{Cre/+}$; *Sik3*$^{Slp\text{-}flox/Slp\text{-}flox}$ mice during the reentrainment LD period after DD. Two-way repeated measure ANOVA. n = 10 for each genotype. Data are mean ± SEM.

$^{Slp\text{-}flox}$ mice showed a shorter circadian period than *Sik3*$^{Slp\text{-}flox/Slp\text{-}flox}$ mice (*Sik3*$^{Slp\text{-}flox/Slp\text{-}flox}$ mice: 23.7 ± 0.1 h and *Vgat*$^{Cre/+}$; *Sik3*$^{Slp\text{-}flox/Slp\text{-}flox}$ mice: 23.4 ± 0.0 h, $P = 0.0243$; Fig. 2 *A* and *D*). These results are opposite to those of *Vgat*$^{Cre/+}$; *Sik3*$^{flox/flox}$ mice. Sleep analysis showed that the arousal peak at ZT11.2 ± 0.3 in *Vgat*$^{Cre/+}$; *Sik3*$^{Slp\text{-}flox/Slp\text{-}flox}$ mice was similar to that of control mice (*SI Appendix*, Fig. S3 *A–C*). The phase-advanced arousal of *Vgat*$^{Cre/+}$; *Sik3*$^{Slp\text{-}flox/Slp\text{-}flox}$ mice was only observed in the wheel-running experiment (Fig. 2*C*). Probably because the phase-advanced activity was easily masked by light, the difference was only detected with the running wheel which enhanced the arousal level and made the interindividual differences smaller (coefficient of variation of activity onset time with wheel running: 0.0274 and arousal peak time from sleep recording: 0.104) (22, 23). A consolidated activity bout at the early dark phase of *Vgat*$^{Cre/+}$; *Sik3*$^{Slp\text{-}flox/Slp\text{-}flox}$ mice was decreased earlier than that of control mice (Fig. 2*B*), suggesting that the light masking affected the beginning of the activity bout. After 3 wk of DD, when LD was resumed at the original circadian timing, activity onset of *Vgat*$^{Cre/+}$; *Sik3*$^{Slp\text{-}flox/Slp\text{-}flox}$ mice was immediately adjusted to the dark phase of LD, as did *Sik3*$^{Slp\text{-}flox/Slp\text{-}flox}$ mice (Fig. 2 *A* and *E*). Thus, *Sik3(Slp)* induction in GABAergic neurons has the opposite effect of SIK3 deficiency in terms of activity onset and circadian period length.

SIK3 Deficiency in NMS-Positive Neurons Caused a Delayed Arousal Peak and a Longer Circadian Period. To further characterize neuronal groups responsible for sleep and circadian behavior changes in *Vgat*$^{Cre/+}$; *Sik3*$^{flox/flox}$ mice, we performed sleep and circadian behavior analysis in *Nms-Cre*-dependent SIK3-deficient mice. NMS-positive neurons account for 40% of SCN neurons and are essential for the pacemaker function of the SCN (5). Similar to *Vgat*$^{Cre/+}$; *Sik3*$^{flox/flox}$ mice, *Nms-Cre; Sik3*$^{flox/flox}$ mice showed a gradual increase in wake time from the dark onset, reaching an arousal peak at ZT14.0 ± 0.6, which was delayed by 2.5 h compared to control mice (same as Fig. 1*A*) (Fig. 3 *A–C* and *SI Appendix*, Fig. S4*A*). Hourly NREM sleep time and REMS time of *Nms-Cre; Sik3*$^{flox/flox}$ mice showed a gradual decrease during the dark phase which was complementary to increased wake time (*SI Appendix*, Fig. S4 *B* and *C*). A delayed arousal peak was also observed under DD (Fig. 3 *D–F* and *SI Appendix*, Fig. S4*I*). *Nms-Cre; Sik3*$^{flox/flox}$ mice showed a second arousal peak at the end of the dark phase similar to control mice under both LD and DD (Fig. 3 *A*, *B*, *D*, and *E*). *Nms-Cre; Sik3*$^{flox/flox}$ mice exhibited total wake time, total NREMS time, total REMS time, mean episode duration of NREMS, and delta power in NREMS similar to control mice under both LD and DD (*SI Appendix*, Fig. S4). Thus, *Nms-Cre; Sik3*$^{flox/flox}$ mice exhibited a delayed peak of arousal in the early dark phase similar to *Vgat*$^{Cre/+}$; *Sik3*$^{flox/flox}$ mice.

Nms-Cre; Sik3$^{flox/flox}$ mice exhibited a longer circadian period than *Sik3*$^{flox/flox}$ mice using a running-wheel activity in DD (*Sik3*$^{flox/flox}$ mice: 23.8 ± 0.1 h and *Nms-Cre; Sik3*$^{flox/flox}$ mice: 24.2 ± 0.1 h, $P = 0.0107$; Fig. 3 *G* and *J*). In LD, *Nms-Cre; Sik3*$^{flox/flox}$ mice showed delayed activity onset with greater variability compared to *Sik3*$^{flox/flox}$ mice (Fig. 3 *G–I*). When LD was resumed at the original circadian timing after 3 wk of DD, the activity onset of *Nms-Cre; Sik3*$^{flox/flox}$ mice quickly adapted to the dark phase of LD (Fig. 3*O*). These results indicate that SIK3 deficiency in NMS-positive neurons is sufficient to reproduce phase-delayed activity/wake during the early dark phase and a longer circadian period in *Vgat*$^{Cre/+}$; *Sik3*$^{flox/flox}$ mice.

***Avp-Cre; Sik3*$^{flox/flox}$ Mice Did Not Show Delayed Arousal Peaks with a Longer Circadian Period.** Next, we examined mice lacking SIK3 in AVP-positive neurons which are a subpopulation of NMS-positive neurons in the SCN (9). In sharp contrast to *Vgat*$^{Cre/+}$; *Sik3*$^{flox/flox}$ mice and *Nms-Cre; Sik3*$^{flox/flox}$ mice, *Avp-Cre; Sik3*$^{flox/flox}$ mice did not show any delay in arousal peak after the onset of the dark phase under LD (Fig. 4 *A–C*) and DD (Fig. 4 *D–F*). *Avp-Cre; Sik3*$^{flox/flox}$ mice showed no change in the total time of wakefulness, NREMS, or REMS (*SI Appendix*, Fig. S5 *A–F*, *I–N*), episode duration of NREMS (*SI Appendix*, Fig. S5 *G–O*), and delta power during NREMS (*SI Appendix*, Fig. S5 *H–P*) under LD and DD.

Circadian behavior analysis using a running wheel showed that *Avp-Cre; Sik3*$^{flox/flox}$ mice had a longer circadian period than *Sik3*$^{flox/flox}$ mice (*Sik3*$^{flox/flox}$ mice: 24.0 ± 0.2 h and *Avp-Cre; Sik3*$^{flox/flox}$ mice: 24.3 ± 0.0 h, $P < 0.0001$; Fig. 4 *G* and *J*). In LD, *Avp-Cre; Sik3*$^{flox/flox}$ mice showed delayed activity onset compared to *Sik3*$^{flox/flox}$ mice by only 0.3 h (Fig. 4 *G–I*). When *Avp-Cre; Sik3*$^{flox/flox}$ mice were released to the original LD after 3 wk of DD, *Avp-Cre; Sik3*$^{flox/flox}$ mice took approximately 7 d before activity onset reached the beginning of the dark phase, whereas the activity onset of *Sik3*$^{flox/flox}$ mice immediately shifted to the beginning of the dark phase (Fig. 4*O*). This result may be because ZT12 on the first day of LD in *Avp-Cre; Sik3*$^{flox/flox}$ and *Sik3*$^{flox/flox}$ mice corresponded to the subjective day and night, respectively, on the last day of DD. Thus, SIK3 deficiency in AVP-positive neurons did not delay arousal peak at the early dark phase but had a longer circadian period.

***Vgat*$^{Cre/+}$; *Sik3*$^{flox/flox}$; *Per2*$^{Luc/Luc}$ Mice Showed Reduced Per2 Amplitude in the SCN.** To examine the effect of SIK3 deficiency on the oscillation of core clock genes in the SCN, we further crossed *Vgat*$^{Cre/+}$; *Sik3*$^{flox/flox}$ mice with *Per2*$^{Luc/Luc}$ mice (24). After the entrainment of *Vgat*$^{Cre/+}$; *Sik3*$^{flox/flox}$; *Per2*$^{Luc/Luc}$ mice and *Sik3*$^{flox/flox}$; *Per2*$^{Luc/Luc}$ mice into LD, SCN slices were dissected during the light phase, and we performed real-time bioluminescence measurements using a charge-coupled device (CCD) camera. The SCN slices from both *Vgat*$^{Cre/+}$; *Sik3*$^{flox/flox}$; *Per2*$^{Luc/Luc}$ mice and *Sik3*$^{flox/flox}$; *Per2*$^{Luc/Luc}$ mice showed robust bioluminescence throughout the recording period (Fig. 5 *A–C*). To compute circadian parameters of bioluminescence, we defined a region of interest (ROI) on both sides of the dorsal and ventral regions of the SCN (Fig. 5*A*), and the sum of the bioluminescence of each ROI was used for further analysis. Bioluminescence of *Vgat*$^{Cre/+}$; *Sik3*$^{flox/flox}$; *Per2*$^{Luc/Luc}$slices steadily oscillated in both the dorsal and ventral parts (Fig. 5 *B* and *C*). There is no statistically significant difference in the bioluminescence period between *Vgat*$^{Cre/+}$; *Sik3*$^{flox/flox}$; *Per2*$^{Luc/Luc}$ slices and that of *Sik3*$^{flox/flox}$; *Per2*$^{Luc/Luc}$ slices (Fig. 5*D*); however, the ventral part of the SCN had a tendency for a shorter period in *Vgat*$^{Cre/+}$; *Sik3*$^{flox/flox}$; *Per2*$^{Luc/Luc}$ mice ($P = 0.1099$, unpaired *t* test). The bioluminescence amplitude was significantly attenuated in *Vgat*$^{Cre/+}$; *Sik3*$^{flox/flox}$; *Per2*$^{Luc/Luc}$ slices, whereas the acrophase and damping factor of *Vgat*$^{Cre/+}$; *Sik3*$^{flox/flox}$; *Per2*$^{Luc/Luc}$ slices were comparable to those of *Sik3*$^{flox/flox}$; *Per2*$^{Luc/Luc}$ slices (Fig. 5 *B*, *C*, *E*, *F*, and *G*). To examine the synchronous oscillation of each cell in the SCN slices, ROIs were redefined to surround each cell in the dorsal or ventral regions of the SCN. Because each cell in the SCN slices from *Vgat*$^{Cre/+}$; *Sik3*$^{flox/flox}$; *Per2*$^{Luc/Luc}$ mice exhibited lower amplitude than *Sik3*$^{flox/flox}$; *Per2*$^{Luc/Luc}$ slices in CCD camera image (Fig. 5*A*), bioluminescence intensities from each cell were normalized by the maximum amplitude of each genotype to confirm the cell oscillation. We investigated that each SCN cell of the *Vgat*$^{Cre/+}$; *Sik3*$^{flox/flox}$; *Per2*$^{Luc/Luc}$ mice synchronously oscillated in both the dorsal and ventral parts of the SCN similar to *Sik3*$^{flox/flox}$; *Per2*$^{Luc/Luc}$ mice (Fig. 5*H*). Thus, SIK3 deficiency in GABAergic neurons attenuated PER2 expression but did not disturb cell synchronicity in SCN slices.

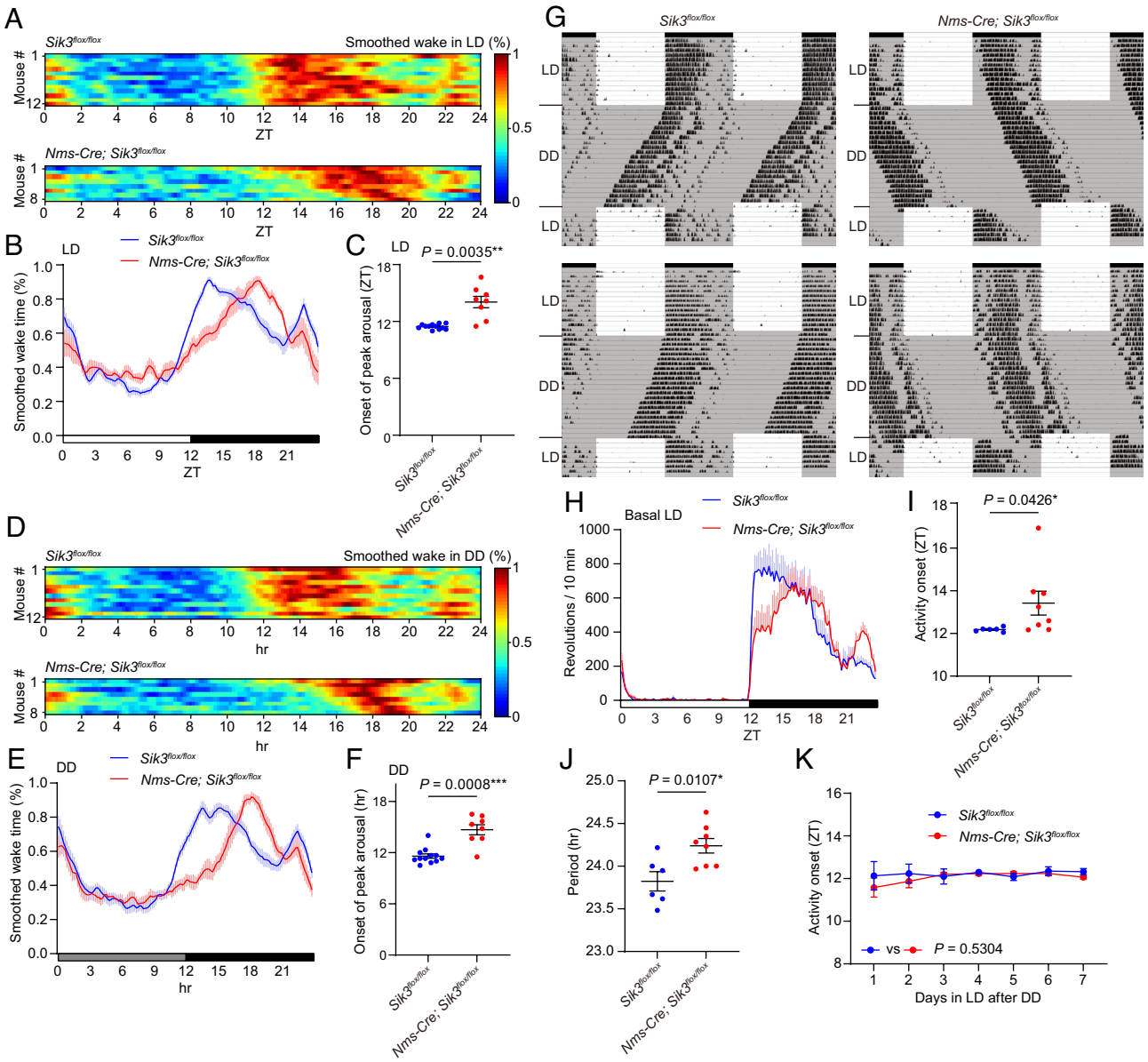

Fig. 3. *Nms-Cre; Sik3*$^{flox/flox}$mice showed phase-delayed awakening at the dark onset and a longer circadian period (*A*) Heat maps of smoothed wake time of individual *Sik3*$^{flox/flox}$ mice and *Nms-Cre; Sik3*$^{flox/flox}$mice in LD. (*B*) Mean of smoothed wake time of *Nms-Cre; Sik3*$^{flox/flox}$mice in LD. (*C*) The onset of peak arousal of *Nms-Cre; Sik3*$^{flox/flox}$mice in LD. Welch's *t* test. (*D*) Heat maps of smoothed wake time of individual *Sik3*$^{flox/flox}$ mice and *Nms-Cre; Sik3*$^{flox/flox}$mice on the first day in DD. (*E*) Mean of smoothed wake time of *Nms-Cre; Sik3*$^{flox/flox}$mice in the first day in DD. (*F*) The onset of peak arousal of *Nms-Cre; Sik3*$^{flox/flox}$mice on the first day in DD. Welch's *t* test. (*G*) Representative double plots of running-wheel activity of a *Sik3*$^{flox/flox}$ mouse and an *Nms-Cre; Sik3*$^{flox/flox}$ mouse. (*H*) Daily wheel revolutions per 10 min of *Nms-Cre; Sik3*$^{flox/flox}$ mice in basal LD. (*I*) Activity onset of *Nms-Cre; Sik3*$^{flox/flox}$ mice in basal LD. Mann–Whitney *U* test. (*J*) Circadian period of *Nms-Cre; Sik3*$^{flox/flox}$ mice. Unpaired *t* test. (*K*) Estimated activity onset of *Nms-Cre; Sik3*$^{flox/flox}$ mice during the reentrainment LD period after DD. Mixed-effects model. For *A–F*, *Nms-Cre; Sik3*$^{flox/flox}$ mice (n = 8) and *Sik3*$^{flox/flox}$ mice (n = 12, same as Fig. 1 *A–F*) were used. For *G–K*, *Nms-Cre; Sik3*$^{flox/flox}$ mice (n = 6) and *Sik3*$^{flox/flox}$ mice (n = 8) were used. Data are mean ± SEM.

***Vgat*$^{Cre/+}$*; Sik3*$^{flox/flox}$ Mice Showed Phase-Delayed Clock Gene Expressions in the Liver.** The SCN synchronizes peripheral oscillators such as liver clocks (1). To examine the effect of SIK3 deficiency in GABAergic neurons on the peripheral core clock gene expressions, we performed qRT-PCR using the mRNA from the liver of *Vgat*$^{Cre/+}$*; Sik3*$^{flox/flox}$ mice harvested on the second day in DD. We confirmed that *Per1*, *Per2, Cry2, Clock, Bmal1,* and *Sik3* were expressed and oscillated in the liver of *Vgat*$^{Cre/+}$*; Sik3*$^{flox/flox}$ mice and *Sik3*$^{flox/flox}$ mice as a control (Fig. 6). To further assess the expression amplitude, acrophase, and period of these genes, we double-plotted the expression level and conducted the cosine fitting (see "qRT-PCR" in the *Materials and Methods*). *Per1* or *Per2* amplitude of *Vgat*$^{Cre/+}$*; Sik3*$^{flox/flox}$ livers was decreased to approximately 55% of *Sik3*$^{flox/flox}$ livers (Fig. 6 *A* and *B*). The period of *Per1*, *Per2, Cry2, Clock,* and *Sik3* was longer in *Vgat*$^{Cre/+}$*; Sik3*$^{flox/flox}$ livers (Fig. 6 *A–D* and *F*). The period of *Bmal1* was comparable between *Vgat*$^{Cre/+}$*; Sik3*$^{flox/flox}$ and *Sik3*$^{flox/flox}$ livers (Fig. 6*E*). The acrophase of all the six genes was phase-delayed in *Vgat*$^{Cre/+}$*; Sik3*$^{flox/flox}$ mice (*Bmal1*: 0.65, *Sik3*: 0.89, *Clock* and *Cry2*: 1.51, *Per1*: 2.26, and *Per2*: 2.28; Fig. 6). These results indicate that SIK3 deficiency in GABAergic neurons induced lower *Per* amplitude and phase-delayed clock gene expression in the liver.

HDAC4 Regulates Circadian Length and Timing of Arousal Peak. SIK3 phosphorylates histone deacetylase 4 (HDAC4), a member of the class IIa histone deacetylase, and enhances cytoplasmic localization of HDAC4, which subsequently changes gene

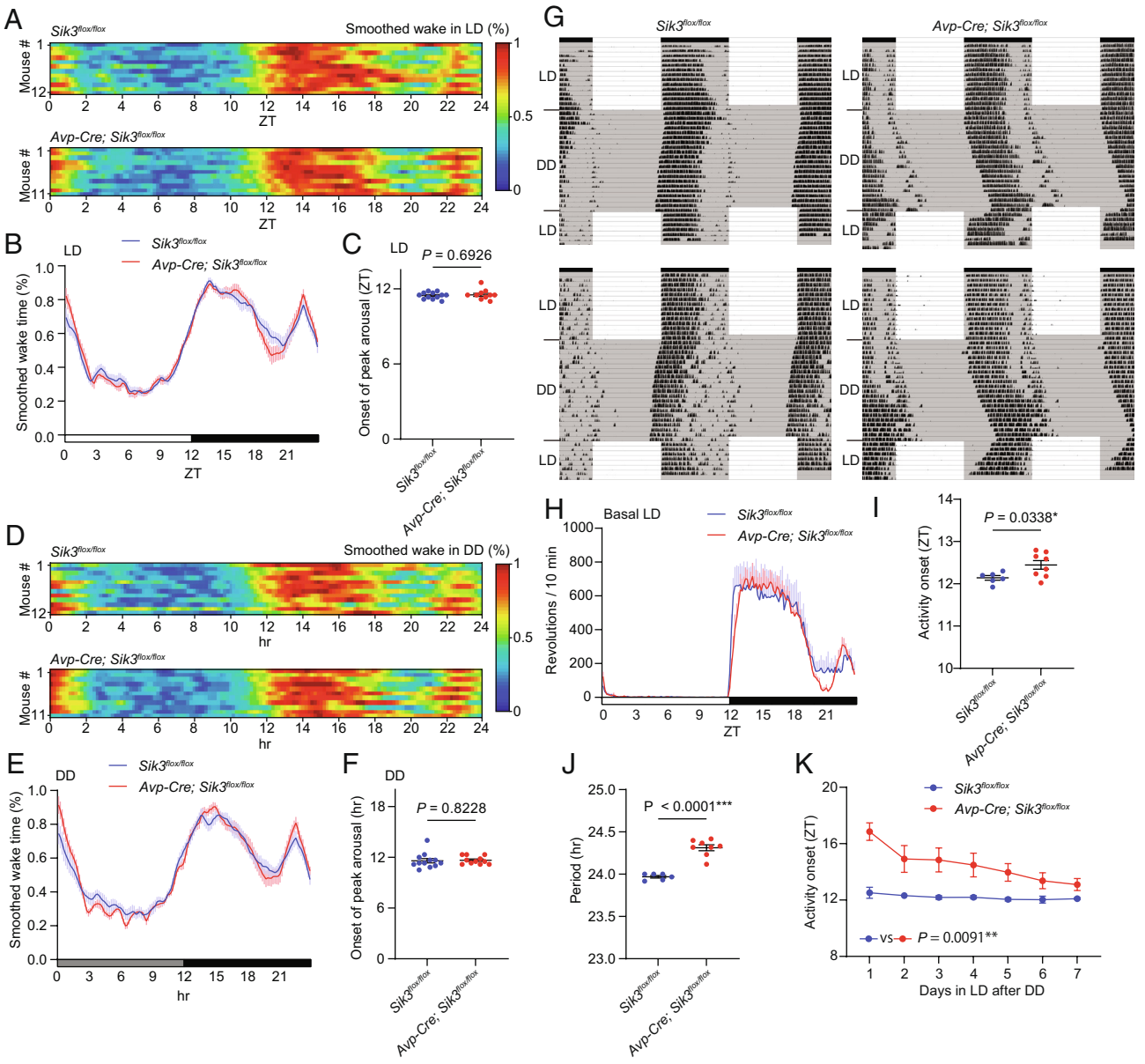

Fig. 4. *Avp-Cre; Sik3*$^{flox/flox}$mice showed a longer circadian period and normal arousal peak (*A*) Heat maps of smoothed wake time of individual *Sik3*$^{flox/flox}$ mice and *Avp-Cre; Sik3*$^{flox/flox}$mice in LD. (*B*) Mean of smoothed wake time of *Avp-Cre; Sik3*$^{flox/flox}$mice in LD. (*C*) The onset of peak arousal of *Avp-Cre; Sik3*$^{flox/flox}$mice in LD. Welch's *t* test. (*D*) Heat maps of smoothed wake time of individual *Sik3*$^{flox/flox}$ mice and *Avp-Cre; Sik3*$^{flox/flox}$mice on the first day in DD. (*E*) Mean of smoothed wake time of *Avp-Cre; Sik3*$^{flox/flox}$mice in the first day in DD. (*F*) The onset of peak arousal of *Avp-Cre; Sik3*$^{flox/flox}$mice on the first day in DD. Welch's *t* test. (*G*) Representative double plots of running-wheel activity of a *Sik3*$^{flox/flox}$ mouse and an *Avp-Cre; Sik3*$^{flox/flox}$ mouse. (*H*) Daily wheel revolutions per 10 min of *Avp-Cre; Sik3*$^{flox/flox}$ mice in basal LD. (*I*) Activity onset of *Avp-Cre; Sik3*$^{flox/flox}$ mice in basal LD. Unpaired *t* test. (*J*) Circadian period of *Avp-Cre; Sik3*$^{flox/flox}$ mice. Unpaired *t* test. (*K*) Estimated activity onset of *Avp-Cre; Sik3*$^{flox/flox}$ mice during the reentrainment LD period after DD. Mixed-effects model. For *A–F*, *Avp-Cre; Sik3*$^{flox/flox}$ mice (n = 11) and *Sik3*$^{flox/flox}$ mice (n = 12, same as Fig. 1 *A–F*) were used. For *G–K*, *Avp-Cre; Sik3*$^{flox/flox}$ mice (n = 6) and *Sik3*$^{flox/flox}$ mice (n = 8) were used.

expression (25–28). Thus, we next assessed the wheel running and sleep/wake behavior of *Hdac4*^{SA} mutant mice, a model of HDAC4 haploinsufficiency (27). *Hdac4*^{SA} has a splice acceptor (SA) mutation in the *Hdac4* gene. The homozygous *Hdac4*^{SA} mutant mice lack HDAC4 protein and exhibit severe abnormality and premature death as reported in HDAC4-deficient mice (27, 29). In the wheel-running experiment, *Hdac4*$^{SA/+}$mice had a shorter behavioral period than *Hdac4*$^{+/+}$mice (*Hdac4*$^{+/+}$mice: 24.0 ± 0.0 h and *Hdac4*$^{SA/+}$mice: 23.7 ± 0.1 h, $P = 0.0235$; Fig. 7 *A–D*), which is opposite of SIK3 deficiency. The activity onset in LD of *Hdac4*$^{SA/+}$mice was similar to that of *Hdac4*$^{+/+}$mice (Fig. 7 *B* and *C*). When LD was resumed at the original circadian timing after DD, the activity onset of *Hdac4*$^{SA/+}$mice was immediately adjusted to the dark phase of LD, as did *Hdac4*$^{+/+}$mice (Fig. 7 *A–E*). Sleep analysis showed that the arousal peak at ZT11.2 ± 0.1 in *Hdac4*$^{SA/+}$mice was similar to that of control mice (*SI Appendix*, Fig. S6 *A–C*). To examine the role of HDAC4 phosphorylation by SIK3, we introduced *Hdac4*^{S245A} mice, in which Ser245, the target serine residue of SIK3, is substituted with alanine (27). Since *Hdac4*^{S245A} mice were too small to move the running wheel smoothly, we only performed a sleep analysis of *Hdac4*^{S245A} mice. The arousal peak of all the control mice was in ZT12 ± 1.5, whereas the arousal peak of five of twenty *Hdac4*$^{S245A/+}$mice exceeded ZT14 (*SI Appendix*, Fig. S6*D*). Consequently, averaged arousal peak of *Hdac4*$^{S245A/+}$mice was significantly delayed to that of *Hdac4*$^{+/+}$mice (*Hdac4*$^{+/+}$mice: ZT11.3 ± 0.0 and *Hdac4*$^{S245A/+}$mice: ZT12.7 ± 0.5, $P = 0.0018$; *SI Appendix*, Fig. S7 *A–C*). These results indicated that HDAC4 regulates the circadian period and arousal peak in a consistent direction with SIK3 activity.

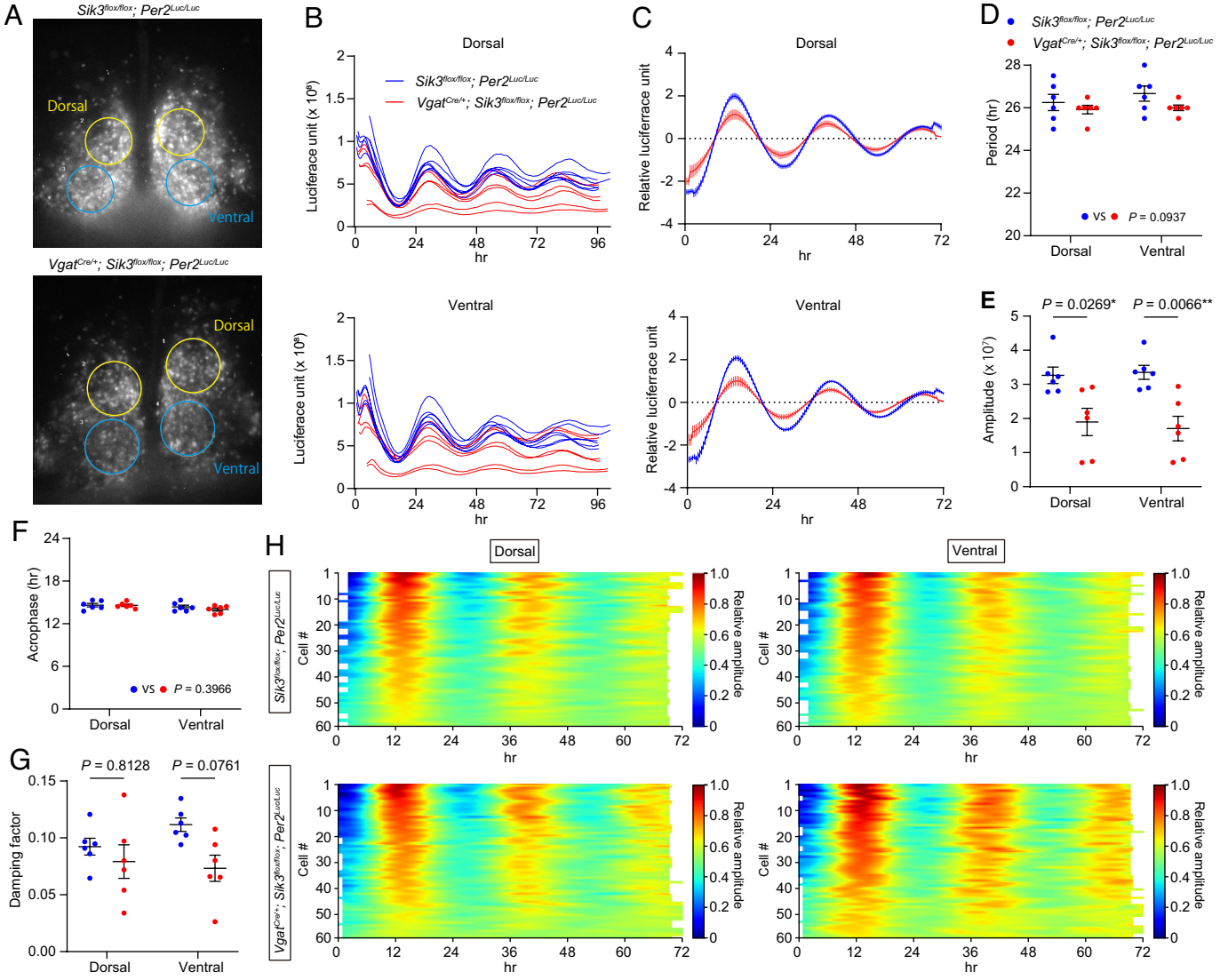

Fig. 5. Bioluminescence rhythms of the SCN explants from *Vgat*$^{Cre/+}$; *Sik3*$^{flox/flox}$; *Per2*$^{Luc/Luc}$ mice (*A*) Representative image of PER2::Luciferase expression of *Vgat*$^{Cre/+}$; *Sik3*$^{flox/flox}$; *Per2*$^{Luc/Luc}$ mice and *Sik3*$^{flox/flox}$; *Per2*$^{Luc/Luc}$ mice at the first peak phase. Four ROIs were defined at the dorsal and ventral regions of a coronal SCN slice. The sum of the bioluminescence intensity in each ROI was calculated and used for further analysis. (*B*) The raw bioluminescence intensities of the SCN explants of *Vgat*$^{Cre/+}$; *Sik3*$^{flox/flox}$; *Per2*$^{Luc/Luc}$ mice. (*C*) Detrended and smoothed bioluminescence of the dorsal or the ventral region in the SCN of *Vgat*$^{Cre/+}$; *Sik3*$^{flox/flox}$; *Per2*$^{Luc/Luc}$ mice. Data were plotted from the next ZT0. (*D–G*) Calculated circadian period length (*D*), amplitude (*E*), acrophase from time point zero (*F*), and damping factor (*G*) of the dorsal or ventral region in the SCN of *Vgat*$^{Cre/+}$; *Sik3*$^{flox/flox}$; *Per2*$^{Luc/Luc}$ mice. Two-way ANOVA followed by Tukey's multiple comparison test. n = 6 in each genotype. Data are mean ± SEM. (*H*) Heat maps of PER2::Luciferase bioluminescence of individual cells in the SCN of *Vgat*$^{Cre/+}$; *Sik3*$^{flox/flox}$; *Per2*$^{Luc/Luc}$ mice. Detrended bioluminescence was normalized by the maximum amplitude in each group. n = 60 in each region and genotype.

Discussion

This study revealed that SIK3 deficiency in GABAergic neurons led to a longer circadian period. Although systemic SIK3-deficient mice have been reported to have a longer circadian period (18), almost all SIK3-deficient mice died, and the surviving few showed severe growth retardation and skeletal and metabolic abnormalities (19, 20). Focusing on the activity of SIK3-deficient mice, they showed fragmented activity bouts even during the light phase (18). In contrast, the activity bouts of SIK3-deficient mice in GABAergic neurons used in this study were consolidated in an active phase similar to wild-type mice, and there were no obvious problems with these mice other than phase-delayed arousal and lengthened circadian period.

Similarly, prolonged circadian periods were found with SIK3 deletion in either NMS-positive neurons or AVP-positive neurons (*Nms-Cre; Sik3*$^{flox/flox}$ mice: 24.2 ± 0.1 hr, *Avp-Cre; Sik3*$^{flox/flox}$ mice: 24.3 ± 0.0 h, and control mice: 23.9 ± 0.1 h). AVP-positive neurons constitute 20% of SCN neurons, and they are also positive for NMS (6). Furthermore, AVP-positive neurons are involved in determining the circadian period (9, 30). It is well known that, when an oscillator with a longer period length is entrained to zeitgeber signals with a shorter period, the phase of the oscillator is delayed from zeitgeber signals (31). Thus, the activity onset in wheel running of both *Nms-Cre; Sik3*$^{flox/flox}$ mice and *Avp-Cre; Sik3*$^{flox/flox}$ mice was phase-delayed. However, phase delay of *Nms-Cre; Sik3*$^{flox/flox}$ mice was more severe than that of *Avp-Cre; Sik3*$^{flox/flox}$ mice (*Nms-Cre; Sik3*$^{flox/flox}$ mice: ZT13.4 ± 0.6, and *Avp-Cre; Sik3*$^{flox/flox}$ mice: ZT12.4 ± 0.1). Furthermore, SIK3 deficiency in NMS-positive neurons resulted in a phase-delayed arousal peak during the early dark phase, but SIK3 deficiency in AVP-positive neurons did not. These results indicated that SIK3 in NMS-positive and AVP-negative neurons is required for robust wakefulness immediately after the light-off, which is independent of wakefulness at the end of the dark phase. Recent single-cell RNA-seq analyses demonstrated that NMS-positive neurons consist of

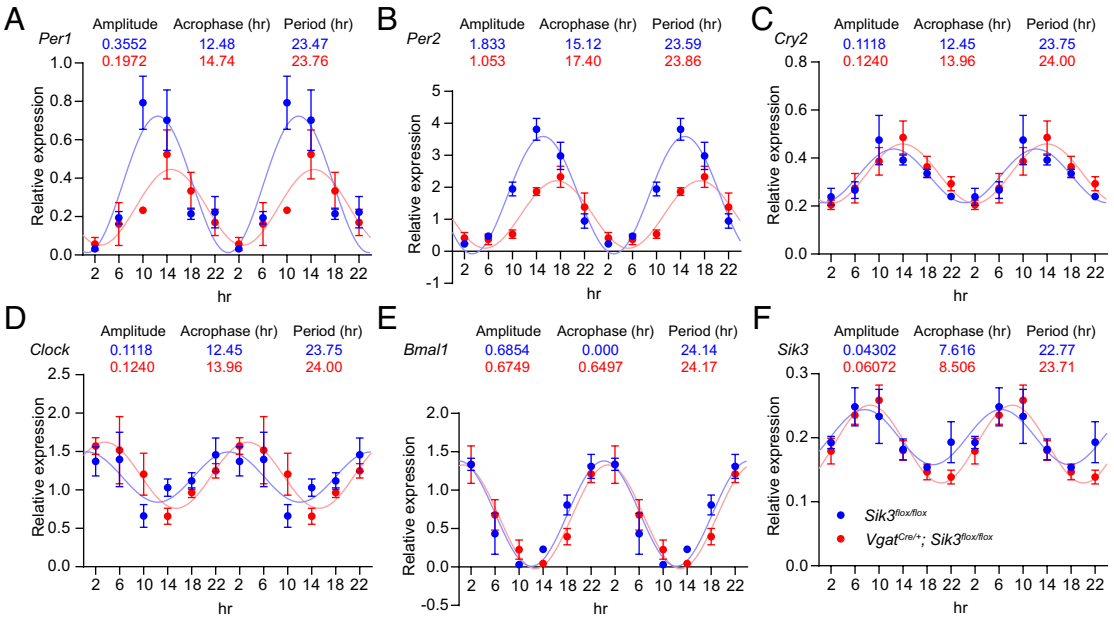

Fig. 6. Core clock gene and *Sik3* expression in the liver from *Vgat*$^{Cre/+}$; *Sik3*$^{flox/flox}$ mice (*A–F*) Relative mRNA expression rhythm of *Per1* (*A*), *Per2* (*B*), *Cry2* (*C*), *Clock* (*D*), *Bmal1*(*E*), and *Sik3* (*F*) of *Vgat*$^{Cre/+}$; *Sik3*$^{flox/flox}$ mice were double-plotted. Pale lines indicated the simulated expression curves of *Vgat*$^{Cre/+}$; *Sik3*$^{flox/flox}$ mice or *Sik3*$^{flox/flox}$ mice. The equation used was y = amplitude*cos(2*pi*(x – acrophase)/period) + baseline. n = 3 in each time point and genotype. Data are mean ± SEM.

AVP-positive neurons and VIP-positive neurons (6, 32). Thus, a delayed arousal peak during the dark phase, which was observed in SIK3 deficiency in NMS-positive neurons but not in SIK3 deficiency in AVP-positive neurons, is thought to be due to SIK3 deficiency in VIP-positive neurons. VIP-positive neurons account for 10% of SCN neurons and are involved in light-mediated circadian phase shift (33) and are required for circadian rhythmicity under DD (32). Furthermore, an intact VIP signaling is required for the circadian period regulation (32, 34–36). Considering the trend that the bioluminescence period was more affected in the ventral part of the SCN by the SIK3 deficiency in GABAergic neurons, it is impossible to reject the possibility that VIP-positive neurons are involved in circadian period length regulation through SIK3 signaling. To investigate in detail the contributions of the subpopulations in the NMS-positive neurons for SIK3-dependent circadian period and arousal timing regulations, further experiments will be useful with mice lacking SIK3 specifically in VIP-positive neurons in the SCN but maintaining normal expression levels of VIP itself.

Genetic manipulations of SIK3 in GABAergic neurons indicate that SIK3 acts to shorten the circadian period length. Since SIK3 phosphorylates HDAC4 and suppresses the nuclear localization of HDAC4 (25, 26), if the SIK3–HDAC4 pathway is involved in circadian behavior control, nuclear HDAC4 may work to lengthen the circadian cycle, which may be reversed when HDAC4 is greatly reduced. As expected, heterozygous

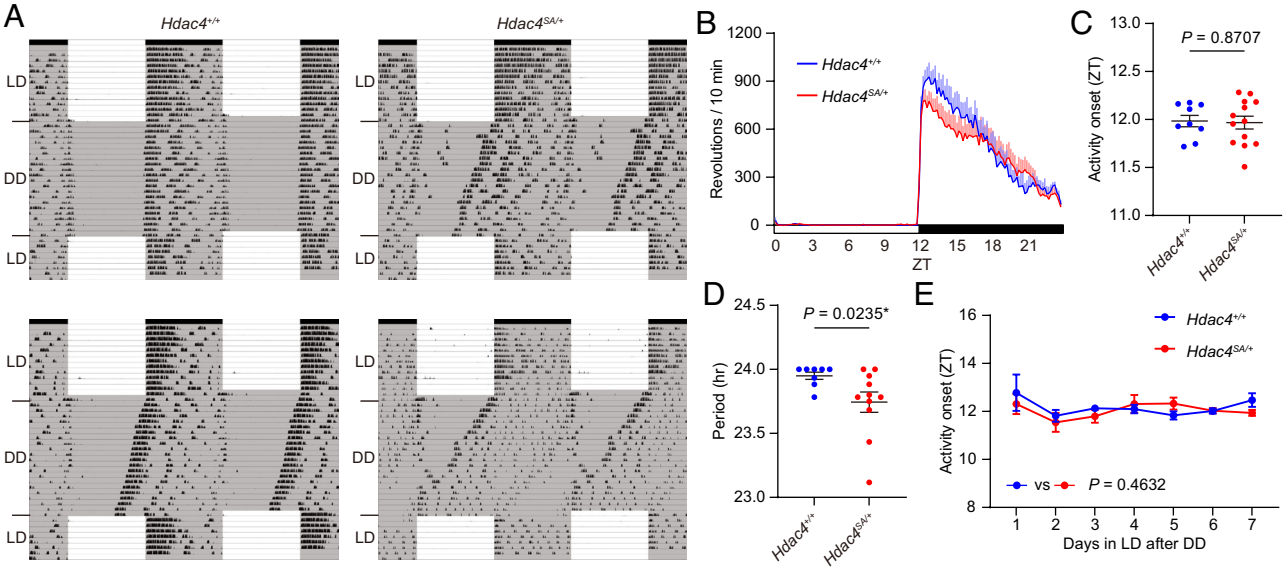

Fig. 7. *Hdac4*$^{SA/+}$ mice showed a shorter circadian period (*A*) Representative double plots of running-wheel activity of a *Hdac4*$^{+/+}$ mouse and a *Hdac4*$^{SA/+}$ mouse. (*B*) Daily wheel revolutions per 10 min of *Hdac4*$^{SA/+}$ mice in basal LD. (*C*) Activity onset of *Hdac4*$^{SA/+}$ mice in basal LD. Unpaired *t* test. (*D*) Circadian period of *Hdac4*$^{SA/+}$ mice. Mann–Whitney *U* test. (*E*) Estimated activity onset of *Hdac4*$^{SA/+}$ mice during the reentrainment LD period after DD. Mixed-effects model. *Hdac4*$^{+/+}$ mice (n = 9) and *Hdac4*$^{SA/+}$ mice (n = 13). Data are mean ± SEM.

HDAC4-deficient mice exhibited a shorter circadian period, whereas mice with a phosphorylation-defective mutation in HDAC4, resistant to phosphorylation by SIK3, showed a delayed arousal peak. In addition, mice deficient in MEF2D, which HDAC4 binds to regulate the expression of target genes, showed a longer circadian period and delayed arousal peak during the onset of the dark phase (37) similar to *Vgat*$^{Cre/+}$*; Sik3*$^{flox/flox}$ mice and *Nms-Cre; Sik3*$^{flox/flox}$ mice. Thus, SIK3–HDAC4 signaling may regulate circadian behavior and arousal peak phase. Recently, NPAS4-deficient mice were reported to show a prolonged circadian period and a delayed or unstable activity onset during LD (38). Since HDAC5, a close paralog of HDAC4 and another substrate of SIK3, can suppress NPAS4 (39), SIK3 may exert its effects on circadian behavior through HDAC4/5–NPAS4. Thus, the SIK3–HDAC4/5 pathway may regulate the circadian period and arousal peak phase through positive transcription regulators like MEF2D and NPAS4.

Core clock genes in the liver of *Vgat*$^{Cre/+}$*; Sik3*$^{flox/flox}$ mice were phase-delayed compared with the control mice in DD. Surprisingly, phase difference and molecular period change were not detected in the SCN explants from *Vgat*$^{Cre/+}$*; Sik3*$^{flox/flox}$*; Per2*$^{Luc/Luc}$ mice, although phase delay in arousal peak was observed in *Vgat*$^{Cre/+}$*; Sik3*$^{flox/flox}$ mice in LD. It is important to note that there is a difference in PER2 protein between experiments, an intact PER2 protein for in vivo behavioral analyses and a PER2::Luciferase fusion protein for SCN explant experiments. SIK3 enhances the phosphorylation and degradation of PER2 directly or indirectly (18). However, PER2::Luciferase signals from the SIK3-deficient SCN were not increased but rather decreased (Fig. 5*B*). A plausible possibility is that PER2::Luciferase fusion protein has a reduced sensitivity to phosphorylation, including that mediated by SIK3 compared with intact PER2. Considering the subtle circadian phenotypes of *Hdac4* mutant mice, SIK3 acts to shorten the circadian period through both a fast PER2 phosphorylation process and relatively slow transcriptional regulation. Also, there remain the possibilities that some non-SCN intrinsic factors mediating the SIK3 pathway–dependent regulation in period length and phase angle may be missing in the SCN explants or that the SCN explants of *Vgat*$^{Cre/+}$*; Sik3*$^{flox/flox}$*; Per2*$^{Luc/Luc}$ mice may exhibit an aftereffect of previous LD (37).

In the SCN, both *Sik1* and *Sik3* are induced by light stimulation (38), and SIK1 is involved in behavioral phase shifts following a jet lag (21). However, SIK3 deficiency in GABAergic neurons did not affect the daily advance of the activity onset after a jet lag. Since *Sik1* is induced 30 min after the light pulse while *Sik3* is induced 3 h later (38), SIK3 has a different role in the light response than SIK1. In addition, SIK1-inactive knock-in mice showed normal behavioral periods (40).

Endogenous SIK3 in the SCN, composed of GABAergic neurons, regulated arousal peak timing and circadian oscillation without affecting total sleep amount and depth. These results replicated the fact that GABAergic neurons do not affect sleep amount or depth via SIK3 (27). Interestingly, the downstream target molecule of SIK3-dependent sleep regulation is HDAC4/5, which is executed by glutamatergic neurons (27, 28). Thus, the SIK3–HDAC4 signaling pathway contributes to the sleep/wake architecture through both processes, sleep homeostasis regulation via glutamatergic neurons and circadian rhythm regulation via GABAergic neurons.

Materials and Methods

Animals. All animal experimental procedures were approved and conducted following the guidelines established by the Institutional Animal Care and Use Committee of the University of Tsukuba (approved protocol ID #22-345). Mice were bred under controlled temperature and humidity conditions (23 ± 2 °C and 55 ± 5% humidity) and maintained on a 12-h light:12-h dark cycle with a white fluorescent lamp as the light source. Food and water access was allowed ad libitum. *Vgat*^{Cre} (*Slc32a1*$^{tm2(cre)Lowl}$/J, Jackson Laboratory #016962, MGI:5141270), *Nms-Cre* (C57BL/6-Tg(Nms-icre)20Ywa/J, Jackson Laboratory #027205, MGI:5638418), *Avp-Cre* (Tg(Avp-icre)#Meid, MGI:5697941), *Per2*^{Luc} (B6.129S6-*Per2*^{tm1Jt}/J, Jackson Laboratory #:006852, MGI:3040876), and *Sik3*$^{Slp\text{-}flox}$ (*Sik3tm2.1Iiis*, MGI:6506974) were used. *Sik3*^{flox} mice, *Hdac4*^{SA}, and *Hdac4*^{S245A} were generated by Kim et al. (27).

Circadian Behavioral Analysis. Instruments for measuring circadian behavior were the same as previously reported (41). Male mice aged 11 to 24 wk old were individually housed in a cage located with a wireless running wheel (Med Associates #ENV-047). The revolutions of wheels were recorded by Wheel Manager software (Med Associates) via a receiving device (Med Associates #DIG807). The mice were habituated to the running wheel under LD for at least 7 d just before recording. Except for *Hdac4*$^{SA/+}$ mice, a green light emitting diode (LED) was used as the light source. The wheel-running experiments of *Hdac4*$^{SA/+}$ mice were conducted under white fluorescent light. Basal revolutions were measured under LD for more than 13 d, and then mice were released into DD for at least 21 d to measure the free-running period. Finally, mice were returned to the original LD for more than 6 d. The revolutions were recorded every minute. Except for *Hdac4*$^{SA/+}$ mice, the circadian period was calculated by χ^2 periodogram from days 7 to 21 in DD. The circadian period of *Hdac4*$^{SA/+}$ mice was calculated using the whole recording days in DD due to the system problem of the wireless receiver that happened during DD. The data from one *Hdac4*$^{+/+}$ mouse and two *Hdac4*$^{SA/+}$ mice were removed because the numbers of recording days were not enough to reach the significance of χ^2 periodogram. The activity onset for wheel running was defined as the time point when the gap of the sum of the total revolutions before and after 6 h from the candidate bins reached the maximum. For the jet lag experiment, a wheel-running behavior was measured under the 12-h light:12-h dark cycle for 10 d followed by 6 h of light advance. Mice were maintained in the shifted light–dark cycles for 10 d. Then, mice were challenged to a 6-h dark delay and wheel-running activity measured for 10 d. The daily shift was calculated by subtracting the mean activity onset during the previous LD from each activity onset after the 6-h light advance. Periodogram computation, activity onset estimation, and actogram visualization were performed using Python.

EEG/EMG Electrode Implantation Surgery. EEG/EMG electrodes containing four electrode pins and two flexible stainless steel wires were implanted into 8- to 10-wk-old male mice as previously described (42, 43). Surgery was performed under stereotaxis control with isoflurane anesthesia (4% for induction and 2% for maintenance). Four electrode pins were implanted at the posterior locations (ML: ±1.27 mm just anterior side of lambdoid sutures) and at 5.03 mm anterior side of the posterior locations. Two ipsilateral pins were used for EEG recording. The electrode was fixed to the skull with dental cement (3M ESPE, RelyX U200 Unicem Syringe Dental Resin Cement), and then, the two EMG wires were inserted into the neck extensor muscles. All mice were allowed at least a 5-d recovery from the surgery. After the recovery period, all mice were housed individually and attached to a tether cable to habituate to the connected condition for more than 7 d. Habituation was performed under the 12-h light:12-h dark cycle with green LED light as the light source, same as the recording condition.

EEG/EMG Recording and Analysis. EEG/EMG recording and analysis were performed as previously described with some modifications (42, 43). EEG/EMG signals were continuously recorded for 48 h, of which the first 24 h was under the 12-h light:12-h dark condition and followed by 24-h constant dark condition. EEG and EMG signals were amplified and filtered (EEG: 0.3 to 300 Hz and EMG: 30 to 300 Hz) with a multichannel amplifier (NIHON KODEN, #AB-611J) and sampled at 250 Hz with an analog-to-digital converter (National Instruments #PCI-6220). The EEG/EMG data were visualized and semiautomatically analyzed by MATLAB-based software followed by visual inspection. A 20-s bin was used to determine wakefulness, NREM sleep, and REM sleep. Wakefulness was scored based on the low-amplitude, fast EEG and vigorous or variable EMG. NREMS was determined based on delta (1 to 4 Hz) frequency dominant, high-amplitude EEG, and low EMG activity. REMS was characterized by theta (6 to 9 Hz) frequency dominant, delta frequency diminished, low-amplitude EEG, and EMG atonia. The total time spent in wakefulness, NREM sleep, and REM sleep was calculated by summing the total number of 20-s bins in each state. NREMS episode durations were computed by dividing the total time spent in NREMS by the number of

NREMS episodes. Epochs with artifacts were included in the time spent analysis but excluded from subsequent spectral analysis. To analyze the EEG spectra, EEG signals were subjected to fast Fourier transform analysis using MATLAB-based custom software, and power spectra of 1 to 30 Hz with 1-Hz bins in each 20-s epoch were calculated. NREMS delta density was the average of the normalized delta power, which was the ratio of delta power to the total EEG power in each epoch of NREMS. To examine the onset of peak arousal, the sum of the wake time in 10-min bin was calculated and then smoothed with 3-h moving average. Smoothed values were normalized by the maximum values in each mouse and then binarized by the mean value of the smoothed wake time. An onset of peak arousal was determined as the latency to the longest consecutive period of threshold exceedance from ZT0 or the beginning of DD. The onset of peak arousal of $Vgat^{Cre/+}$; $Sik3^{+/+}$mice, $Vgat^{Cre/+}$; $Sik3^{Slp\text{-}flox/+}$mice, $Vgat^{Cre/+}$; $Sik3^{Slp\text{-}flox/Slp\text{-}flox}$mice, $Hdac4^{+/+}$ mice, $Hdac4^{SA/+}$ mice, and $Hdac4^{S245A/+}$ mice was reanalyzed using the data in Kim et al. (27).

SCN Slice Culture and Bioluminescence Analysis. $Vgat^{Cre/+}$; $Sik3^{flox/flox}$; $Per2^{Luc/Luc}$ mice and $Sik3^{flox/flox}$; $Per2^{Luc/Luc}$ mice were used. Mice were maintained in the 12-h light:12-h dark cycle with a white fluorescent lamp as the light source. Male mice aged 14 to 22 wk old were harvested between ZT5 and ZT10. Then, 150-μm-thick coronal brain slices were prepared using Vibratome (Leica VT1200S). A pair of mid-rostrocaudal SCN were dissected and cultured at 37 °C on a Millicell Cell Culture Insert (Millipore PICM0RG50) in a sealed 35-mm dish containing 1.5 mL recording medium (phenol red–free DMEM (SIGMA D2902), 10 mM HEPES, and 3.5 g/L D-glucose, pH 7.0) supplemented with 0.42 mM $NaHCO_3$, 1% penicillin–streptomycin (Wako 168-23191), 2% B-27 supplements (Gibco), and 0.2 mM D-luciferin potassium salt (Wako). Bioluminescence from the SCN slices was detected using a CCD camera (Cellgraph, AB-3000D) at a 20-min exposure time with a 10-min interval for 4 d. One SCN slice from $Vgat^{Cre/+}$; $Sik3^{flox/flox}$; $Per2^{Luc/Luc}$ mice was excluded from further analysis because it only covered the posterior edge of the SCN and bioluminescence faded during recording. Four points of ROI were defined in the dorsal medial and ventral medial parts of one pair of the SCN slice. The sum of the bioluminescence intensity in each ROI was calculated and accompanied by circadian parameter computation using Python. Bioluminescence values were detrended by subtracting 24-h moving average values, and then data were smoothened with a Savitzky–Golay filter (12-h window, cubic polynomial) in SciPy. Values from the next ZT0 were used for analysis. The middle of the time points in which the smoothed values crossed value 0 upward and downward was defined as peak phases as previously reported (44). Significant oscillation was defined as a 6-h mean value of around the first peak that was two SD further than the average of detrended values. The period was calculated as the difference between two adjacent peak phases. The amplitude was the sum of the absorbed value of the first peak and the subsequent trough. The acrophase was defined as the latency to the first peak from ZT0. The damping factor was calculated using the values of the first peak and the second peak.

To confirm the synchronization of individual cells, forty points of circular ROI were redefined in the SCN slice (20 ROIs in the dorsal part and 20 ROIs in the ventral part). ROIs enclosed one cell at the beginning of the successive image; however, ROIs were not traced to each cell because it was hard to distinguish one cell from others due to the high density of cells and fading luminescence. Bioluminescence from each ROI was normalized with the maximum value of each group and visualized as the heat map using Python.

qRT-PCR. Livers of 9- to 14-wk-old male mice were harvested at the specific time of the second day under DD. Total RNA was prepared using Lipid Tissue Mini Kit (Qiagen) and QIAzol Lysis Reagent (Qiagen) according to the manufacturer's protocol. Total RNA was reverse-transcribed with an oligo dT primer and PrimeScript Reverse Transcriptase Kit (TaKaRa). Synthesized cDNA was subjected to real-time PCR (ViiA7; ThermoFisher) using TB Green Premix Ex Taq II (TaKaRa) and gene-specific primers. The expression levels were normalized with the *glyceraldehyde-3-phosphate dehydrogenase* (*Gapdh*) gene. The primers used were *Per1, Clock, Bmal1, Cry2* (ref. 45), *Per2*-Fw (5′-GTGTT GAAGG AGGAC CAGGA-3′), *Per2*-Rv (5′-AAACA CAGCC TGTCA CATCG), *Sik3*-Fw (5′-AGCGC CAGTC AGATT CAGAT-3′), *Sik3*-Rv (5′-CGTAG TTGGC AGGGG AGAA-3′), *Gapdh*-Fw (5′-AGAAC ATCAT CCCTG CATCC-3′), and *Gapdh*-Rv (5′-CACAT TGGGG GTAGG AACAC-3′).

To calculate the wavelength, acrophase, and amplitude, mRNA expression levels were double-plotted, and cosine fitting was performed using a customized nonlinear regression method in GraphPad Prism 9.3.1. The equation used was y = amplitude*cos(2*pi*(x – acrophase)/period) + baseline, and the equation satisfies the following conditions: period > 22, amplitude > 0, and baseline > 0. The acrophase range was $0 \leqq \text{acrophase} < 24$. The goodness of fitting was assessed by R squared.

Statistical Analysis. Two-way ANOVA or two-way repeated measure ANOVA was used for two-factor data. Mixed-effects model was applied for the two-factorial repeated measured data with missing values instead of the two-way repeated measure ANOVA. In pairwise comparison, we first visually confirmed normality and homoscedasticity of the data through the plot. An unpaired *t* test was used for the pairwise comparison with normal distribution and equal variance. The Mann–Whitney *U* test was applied if the data seemed not to follow Gaussian distribution. When the data followed Gaussian distribution but the variance was not equal, we used two-tailed Welch's *t* test. Tukey's multiple comparisons were used for multiple comparisons. $P < 0.05$ was considered statistically significant. All data were expressed as mean with SEM. Graph visualization and statistical analyses were performed using GraphPad Prism 9.3.1.

Data, Materials, and Software Availability. All study data are included in the article and/or *SI Appendix*. Source data to support these findings are available in figshare (https://doi.org/10.6084/m9.figshare.22138214.v1) (46). The python scripts used in this paper are available on GitHub (https://github.com/fuyuki-asano/circadian_analysis) (47).

ACKNOWLEDGMENTS. We thank Hitoshi Okamoto from RIKEN Center for Brain Science (CBS)-Kao Collaboration Center for contribution to *Avp-Cre* mice generation, Joseph S. Takahashi from the University of Texas Southwestern Medical Center for discussing the data, all Y/F laboratory members and International Institute for Integrative Sleep Medicine (IIIS) members, especially Takehiro Miyazaki, and Kumi Ebihara for technical support. This work was supported by the World Premier International Research Center Initiative (WPI) from Ministry of Education, Culture, Sports, Science and Technology (MEXT) to M.Y., Japan Society for the Promotion of Science (JSPS) Grants-in-Aid for Scientific Research (KAKENHI) (17H06095 and 22H04918 to M.Y. and H.F.; 17H04023, 17H05583, and 20H00567 to H.F.; 26507003 and 18968064 to C.M. and H.F.; 15J00393 and 18J21517 to F.A., and 18K14811 to T.F.), Japan Science and Technology Agency (JST) Core Research for Evolutional Science and Technology (CREST) (JPMJCR1655 to M.Y.), Japan Agency for Medical Research and Development (AMED) (JP21zf0127005 to M.Y.), JSPS DC2 17J07957 to S.J.K., University of Tsukuba Basic Research Support Program Type A to S.J.K., and Funding Program for World-Leading Innovative R&D on Science and Technology (FIRST Program) from JSPS to M.Y.

Author affiliations: [a]International Institute for Integrative Sleep Medicine, University of Tsukuba, Tsukuba 305-8575, Japan; [b]Laboratory Animal Resource Center in Transborder Medical Research Center, Institute of Medicine, University of Tsukuba, Tsukuba 305-8575, Japan; [c]Department of Integrative Neurophysiology, Graduate School of Medical Sciences, Kanazawa University, Kanazawa 920-8640, Japan; [d]Institute of Medicine, University of Tsukuba, Tsukuba 305-8575, Japan; [e]Department of Anatomy, Toho University Graduate School of Medicine, Tokyo 143-8540, Japan; [f]Department of Molecular Genetics, University of Texas Southwestern Medical Center, Dallas, TX 75390; and [g]Life Science Center for Survival Dynamics, Tsukuba Advanced Research Alliance, University of Tsukuba, Tsukuba 305-8577, Japan

1. J. A. Mohawk, C. B. Green, J. S. Takahashi, Central and peripheral circadian clocks in mammals. *Annu. Rev. Neurosci.* **35**, 445–462 (2012).
2. M. H. Hastings, E. S. Maywood, M. Brancaccio, Generation of circadian rhythms in the suprachiasmatic nucleus. *Nat. Rev. Neurosci.* **19**, 453–469 (2018).
3. L. Yan, Expression of clock genes in the suprachiasmatic nucleus: effect of environmental lighting conditions. *Rev. Endocr. Metab. Disord.* **10**, 301–310 (2009).
4. E. D. Herzog, T. Hermanstyne, N. J. Smyllie, M. H. Hastings, Regulating the suprachiasmatic nucleus (SVN) circadian clockwork: Interplay between cell-autonomous and circuit-level mechanisms. *Cold Spring Harb. Perspect. Biol.* **9**, a027706 (2017).
5. I. T. Lee *et al.*, Neuromedin s-producing neurons act as essential pacemakers in the suprachiasmatic nucleus to couple clock neurons and dictate circadian rhythms. *Neuron* **85**, 1086–1102 (2015).

6. S. Wen *et al.*, Spatiotemporal single-cell analysis of gene expression in the mouse suprachiasmatic nucleus. *Nat. Neurosci.* **23**, 456–467 (2020).
7. E. S. Maywood, J. E. Chesham, J. A. O'Brien, M. H. Hastings, A diversity of paracrine signals sustains molecular circadian cycling in suprachiasmatic nucleus circuits. *Proc. Natl. Acad. Sci. U.S.A.* **108**, 14306–14311 (2011).
8. Y. Yamaguchi *et al.*, Mice genetically deficient in vasopressin V1a and V1b receptors are resistant to jet lag. *Science* **342**, 85–90 (2013).
9. M. Mieda *et al.*, Cellular clocks in AVP neurons of the SCN are critical for interneuronal coupling regulating circadian behavior rhythm. *Neuron* **85**, 1103–1116 (2015).
10. M. D. Edwards, M. Brancaccio, J. E. Chesham, E. S. Maywood, M. H. Hastings, Rhythmic expression of cryptochrome induces the circadian clock of arrhythmic suprachiasmatic nuclei through arginine vasopressin signaling. *Proc. Natl. Acad. Sci. U.S.A.* **113**, 2732–2737 (2016).
11. D. Ono, K.-I. Honma, S. Honma, Roles of neuropeptides, VIP and AVP, in the mammalian central circadian clock. *Front. Neurosci.* **15**, 650154 (2021).
12. D. Ono *et al.*, The mammalian circadian pacemaker regulates wakefulness via CRF neurons in the paraventricular nucleus of the hypothalamus. *Sci. Adv.* **6**, eabd0384 (2020).
13. B. Collins *et al.*, Circadian VIPergic neurons of the suprachiasmatic nuclei sculpt the sleep-wake cycle. *Neuron* **108**, 486–499.e5 (2020).
14. J. S. Takahashi, Transcriptional architecture of the mammalian circadian clock. *Nat. Rev. Genet.* **18**, 164–179 (2017).
15. H. Funato *et al.*, Forward-genetics analysis of sleep in randomly mutagenized mice. *Nature* **539**, 378–383 (2016).
16. T. Honda *et al.*, A single phosphorylation site of SIK3 regulates daily sleep amounts and sleep need in mice. *Proc. Natl. Acad. Sci. U.S.A.* **115**, 10458–10463 (2018).
17. K. Iwasaki *et al.*, Induction of mutant *Sik3*^{Sleepy} allele in neurons in late infancy increases sleep need. *J. Neurosci.* **41**, 2733–2746 (2021), 10.1523/JNEUROSCI.1004-20.2020.
18. N. Hayasaka *et al.*, Salt-inducible kinase 3 regulates the mammalian circadian clock by destabilizing PER2 protein. *Elife* **6**, e24779 (2017).
19. T. Uebi *et al.*, Involvement of SIK3 in glucose and lipid homeostasis in mice. *PLoS One* **7**, e37803 (2012).
20. S. Sasagawa *et al.*, SIK3 is essential for chondrocyte hypertrophy during skeletal development in mice. *Development* **139**, 1153–1163 (2012).
21. A. Jagannath *et al.*, The CRTC1-SIK1 pathway regulates entrainment of the circadian clock. *Cell* **154**, 1100–1111 (2013).
22. D. M. Edgar, T. S. Kilduff, C. E. Martin, W. C. Dement, Influence of running wheel activity on free-running sleep/wake and drinking circadian rhythms in mice. *Physiol. Behav.* **50**, 373–378 (1991).
23. L. Milinski *et al.*, Waking experience modulates sleep need in mice. *BMC Biol.* **19**, 65 (2021).
24. S.-H. Yoo *et al.*, PERIOD2::LUCIFERASE real-time reporting of circadian dynamics reveals persistent circadian oscillations in mouse peripheral tissues. *Proc. Natl. Acad. Sci. U.S.A.* **101**, 5339–5346 (2004).
25. D. R. Walkinshaw *et al.*, The tumor suppressor kinase LKB1 activates the downstream kinases SIK2 and SIK3 to stimulate nuclear export of class IIa histone deacetylases. *J. Biol. Chem.* **288**, 9345–9362 (2013).
26. S.-Y. Park, J.-S. Kim, A short guide to histone deacetylases including recent progress on class II enzymes. *Exp. Mol. Med.* **52**, 204–212 (2020).
27. S. J. Kim *et al.*, Kinase signalling in excitatory neurons regulates sleep quantity and depth. *Nature* **612**, 512–518 (2022), 10.1038/s41586-022-05450-1.
28. R. Zhou *et al.*, A signalling pathway for transcriptional regulation of sleep amount in mice. *Nature* **612**, 519–527 (2022), 10.1038/s41586-022-05510-6.
29. R. B. Vega *et al.*, Histone deacetylase 4 controls chondrocyte hypertrophy during skeletogenesis. *Cell* **119**, 555–566 (2004).
30. M. Mieda, H. Okamoto, T. Sakurai, Manipulating the cellular circadian period of Arginine Vasopressin neurons alters the behavioral circadian period. *Curr. Biol.* **26**, 2535–2542 (2016).
31. J. Aschoff, *Endocrine Rhythms* (Krieger Raven Press, 1979).
32. W. D. Todd *et al.*, Suprachiasmatic VIP neurons are required for normal circadian rhythmicity and comprised of molecularly distinct subpopulations. *Nat. Commun.* **11**, 4410 (2020).
33. J. R. Jones, T. Simon, L. Lones, E. D. Herzog, SCN VIP neurons are essential for normal light-mediated resetting of the circadian system. *J. Neurosci.* **38**, 7986–7995 (2018).
34. C. S. Colwell *et al.*, Disrupted circadian rhythms in VIP- and PHI-deficient mice. *Am. J. Physiol.-Regul. Integr. Comp. Physiol.* **285**, R939–R949 (2003).
35. A. H. Cheng, S. W. Fung, H.-Y.M. Cheng, Limitations of the Avp-IRES2-Cre (JAX #023530) and VIP-IRES-Cre (JAX #010908) models for chronobiological investigations. *J. Biol. Rhythms* **34**, 634–644 (2019).
36. D. A. M. Joye *et al.*, Reduced VIP expression affects circadian clock function in VIP-IRES-CRE mice (JAX 010908). *J. Biol. Rhythms* **35**, 340–352 (2020).
37. J. A. Mohawk *et al.*, Neuronal myocyte-specific enhancer factor 2D (MEF2D) is required for normal circadian and sleep behavior in mice. *J. Neurosci.* **39**, 7958–7967 (2019).
38. P. Xu *et al.*, NPAS4 regulates the transcriptional response of the suprachiasmatic nucleus to light and circadian behavior. *Neuron* **109**, 3268–3282.e6 (2021), 10.1016/j.neuron.2021.07.026.
39. M. Taniguchi *et al.*, HDAC5 and its target gene, Npas4, function in the nucleus accumbens to regulate cocaine-conditioned behaviors. *Neuron* **96**, 130–144.e6 (2017).
40. L. Taylor *et al.*, Light regulated SIK1 remodels the synaptic phosphoproteome to induce sleep. bioRxiv [Preprint] (2021), https://doi.org/10.1101/2021.09.28.462159 (Accessed 17 February 2022).
41. M. Park *et al.*, Loss of the conserved PKA sites of SIK1 and SIK2 increases sleep need. *Sci. Rep.* **10**, 1–14 (2020).
42. C. Miyoshi *et al.*, Methodology and theoretical basis of forward genetic screening for sleep/wakefulness in mice. *Proc. Natl. Acad. Sci. U.S.A.* **116**, 16062–16067 (2019).
43. K. Iwasaki, N. Hotta-Hirashima, H. Funato, M. Yanagisawa, Protocol for sleep analysis in the brain of genetically modified adult mice. *STAR Protoc.* **2**, 100982 (2021).
44. T. Maejima *et al.*, GABA from vasopressin neurons regulates the time at which suprachiasmatic nucleus molecular clocks enable circadian behavior. *Proc. Natl. Acad. Sci. U.S.A.* **118**, e2010168118 (2021).
45. A. Hirano *et al.*, In vivo role of phosphorylation of cryptochrome 2 in the mouse circadian clock. *Mol. Cell. Biol.* **34**, 4464–4473 (2014).
46. F. Asano *et al.*, SIK3–HDAC4 in the suprachiasmatic nucleus regulates the timing of arousal at the dark onset and circadian period in mice. Figshare. https://figshare.com/ndownloader/articles/22138214/versions/1. Deposited 22 February 2023.
47. F. Asano. Circadian Analysis. GitHub. https://github.com/fuyukiasano/circadian_analysis/archive/refs/heads/master.zip. Deposited 24 February 2022.